C. J. McMahon, Jr., C. L. Briant and S. K. Banerji

Fracture 1977, Volume 1, ICF4, Waterloo, Canada, June 19 - 24, 1977

THE EFFECTS OF HYDROGEN AND IMPURITIES ON BRITTLE FRACTURE IN STEEL

C. J. McMahon, Jr*, C. L. Briant** and S. K. Banerji***

ABSTRACT

Recent experimental work on the relationship between impurity-induced embrittlement and hydrogen-induced cracking in high strength and ultra high strength steels is reviewed. It is shown that, as the intergranular concentration of embrittling impurities increases, the intergranular cohesive strength and the threshold stress intensity for hydrogen-induced cracking decrease, and the mode shifts from cleavage toward intergranular. A preliminary model of brittle crack formation in steel is described which attempts to rationalize the hydrogen and impurity effects in terms of both their respective influences on the cohesive strength of iron and the stress field ahead of a crack when local yielding has occurred.

INTRODUCTION

Brittle fracture of steel can be induced by two types of segregation of solute elements. One is the segregation of impurities to grain boundaries during heat treatment or high temperature service; the other is the segregation of absorbed hydrogen to regions of high lattice expansion resulting from an applied stress. The effects of impurities and hydrogen can be superimposed and can lead to intergranular cracking at exceedingly low values of applied stress or stress intensity. In this paper we review our present knowledge of this phenomenon and consider the development of a criterion for brittle cracking in the presence of impurity and hydrogen effects.

EMBRITTLEMENT BY IMPURITIES

It is well established that solute elements from Groups IV to VI (cf. Table 1), usually present as residual impurities, can segregate to grain boundaries in steels, reduce intergranular cohesion, and cause a shift in fracture mode from strain-induced microvoid coalescence to stress-induced intergranular cracking. This is most easily observed as an increase in the notched-bar tough-to-brittle transition temperature.

Group VI elements are highly surface active in Fe and very potent as embrittling solutes [1,2,3]. Elements from Groups IV and V segregate less strongly in Fe and are less potent in lowering cohesion; however, they

*Department of Metallurgy and Materials Science, University of Pennsylvania.
**General Electric Company, Corporate Research and Development, Schenectady, New York, 12301.
***Foote Mineral Company, Exton, Pennsylvania, 19341.

can interact with alloy elements (e.g., Ni and Mn [4,5]) such that substantial cosegregation of alloy and impurity elements occurs and severe embrittlement can result. Other elements can apparently enhance segregation without segregating themselves (e.g., Cr [6]) or can act as scavengers and eliminate segregation (e.g., Ti, Mo [7,8]) of specific impurities. These effects are summarized in Table 1. Increases in matrix strength and grain size exacerbate the effects of the embrittling impurities [6]. This subject has been reviewed recently [9,10] and will not be treated in detail here.

EMBRITTLEMENT BY HYDROGEN

There is abundant experimental evidence that hydrogen, when absorbed into the bcc Fe lattice in sufficient quantity, can act to lower the cohesive strength of the lattice. Hydrogen is a special kind of embrittling solute because of its extraordinary high mobility in bcc Fe at ambient temperatures. In any nonuniformly stressed solid there is a driving force for solute migration which depends on the atomic volume of the solute and the gradient in the hydrostatic component of the applied stress. Thus, hydrogen in steel tends to collect in regions of large hydrostatic tension.† Because of its mobility (D_H in Fe $\simeq 10^{-2} m^2 s^{-1}$ at 300 K) [11] and its cohesion-lowering properties, its effects can be devastating in alloy steels.††

There appears to be general agreement that hydrogen can be absorbed into steel if it becomes adsorbed onto a bare metallic surface when the steel is stressed in an aqueous medium or in a hydrogen-containing gas. The bare surface can be produced when a surface film is broken by an emerging slip step. Hydrogen-induced cracking in alloy steels with yield strength $> \sim 600$ MPa (~ 90 ksi) is often observed to occur along prior austenitic grain boundaries; this suggests that the influence of segregated impurities may be important. Hence, one should include impurity effects if a complete understanding of the behavior of hydrogen is to be achieved. We consider first some experimental results obtained in an acidic aqueous solution and then some more recent experiments in H_2 gas. These results have been used as a guide for the construction of a model of the fracture process.

Hydrogen-Induced Cracking in an H_2SO_4 Solution.

The effects of segregated impurities on hydrogen-induced cracking of a high strength steel was first studied by Cabral et al. [14], who found that the threshold stress for cracking of smooth specimens of a Ni-Cr steel in an H_2SO_4 solution decreased significantly when the tempered steel was aged at 773 K. The cracking mode changed from transgranular to intergranular as a result of the ageing treatment.

†Hydrogen also tends to precipitate in voids and, when its fugacity is high, as in cathodic charging experiments, the internal pressure can be large enough to cause void growth and cracking. This is outside the scope of our present consideration, which is concerned with lower fugacity ranges and the effects of applied stress.

††Note that nitrogen is also an embrittling element in Fe [12] and has some mobility (D_N in Fe $\simeq 10^{-12} m^2 s^{-1}$ at 300 K [13]). If present in solution in steels, it should exhibit the same tendency as hydrogen, but on a much-reduced scale.

A subsequent study by Yoshino and McMahon [15] on a 5% NiCrMoV steel (HY130) utilized pre-cracked specimens in the same environment and produced similar results in terms of the threshold stress intensity K_{th} for crack growth. Auger analysis [16] of grain boundaries broken open in ultra high vacuum showed the major intergranular impurity in the steel embrittled by step cooling to be Si, with smaller amounts of P and N. The cracking behavior was characterized by a "static fatigue" type of plot, as shown in Figure 1. It is interesting to note that step cooling produced reductions of K_c in air and K_{th} in H_2SO_4 which were equivalent. That is, the difference between K_c in air and K_{th} in H_2SO_4 was the same in the unembrittled and the step-cooled conditions. This seems to imply that the impurity and hydrogen effects were separable and additive. However, this may be only fortuitous, since the fracture of the unembrittled steel in air occurred by microvoid coalescence, whereas the others occurred by brittle modes. Ultimately, we wish to determine under what conditions the hydrogen effect can be simply added to other solute effects and when these effects interact non-additively.

Hydrogen-Induced Cracking in a Gaseous Environment

There are certain experimental difficulties in the study of hydrogen-induced cracking in aqueous media, not the least of which are the uncertainties about the complicated surface reactions and the electrochemical conditions inside the crack. Experiments done in H_2 gas should give information on the hydrogen-impurity interactions that can be interpreted more readily, since gas pressure can be used to control the equilibrium solubility of hydrogen in the lattice at any temperature. Hence, we have adopted the technique of determining the crack growth rate v as a function of the stress intensity factor K, employing bolt-loaded WOL specimens [17] stressed to a fixed displacement in H_2 at a controlled temperature and pressure.† The v-K curve is generally plotted with v on a log scale and tends to exhibit three stages [18,19]: (I) a rapid rise in log v from a threshold K value, denoted here as K_{th}, (II) a second stage in which log v sometimes appears to be invariant with increasing K, and (III) a final stage of acceleration as cracking tends towards instability at $K \simeq K_c$. Depending on how close K_c is to K_{th}, stage II may appear only as an inflection in the log v vs K curve, as indicated by Figure 2.

The semi-log v-K plot is used for convenience, because it facilitates the identification of a K_{th} (defined at an arbitrarily low v) and because a large range of v fits on a small piece of paper. However, such a plot has no known functional significance, and it may be seriously misleading if one attempts to treat stage II as a steady state. The measured crack length does not generally vary smoothly with time, and the scatter in the derived v vs K data is generally large; the log v vs K plot masks this scatter [20].

High Strength Steels

The same heat of HY130 steel used by Yoshino and McMahon [15] was utilized to begin the study of cracking in H_2 gas [20]. The impurity effects were characterized by notched-bar tests and Auger electron spectroscopy of intergranular fracture surfaces, as shown in Figure 3. As a result of ageing at 480°C, the transition temperature increased significantly, generally in proportion to the intergranular concentration of Si. The grain

†Rising K tests of compact tension specimens in a controlled hydrogen environment were also used.

boundaries also became enriched in N and P, as well as Ni and Mn. The latter two elements are believed to act as promoters of segregation of embrittling elements by cosegregation (cf. Table 1), rather than as embrittling elements themselves [9].

The effects of the variation of grain boundary composition on the v-K curve are shown in Figure 4. Values of K_{th} and v_{II} are strongly affected; v_{II} is taken to be the region of the first inflection in the steeply-rising v-K curve above K_{th}. As shown in Figure 5 K_{th} decreases and v_{II} increases, with increasing ageing time. It is important to note that the mode of cracking in hydrogen in the unembrittled steel is cleavage, as opposed to the microvoid coalescence found in air. That is, H_2 promotes cleavage fracture when impurity effects are absent.

Ultra High Strength Steels

As the prototypical material in this category we have chosen the often-studied 4340-type steel [21]. Here the impurity effects manifest themselves in what is perhaps most aptly referred to as one-step temper embrittlement [22]. A toughness trough occurs in the room temperature fracture energy of a notched-bar impact specimen when plotted against the temperature of tempering (which is the one embrittlement step). Figure 6 illustrates the toughness troughs in 4 different commercial heats of 4340 steel, and the absence of such a trough in a 4340-type high purity vacuum-induction melted steel which received the same heat treatment and had the same strength. The toughness troughs in the commercial steels were accompanied by corresponding peaks in the amount of intergranular fracture; only a very small amount of intergranular fracture could be produced in the high purity steel. It is well established that the onset of the trough coincides with the formation of M_3C carbides [23,24]. Apparently the tendency for impurity-induced intergranular fracture (which also occurs in as-quenched impure steels) is accentuated by carbide formation in the prior austenitic grain boundaries. It is thought that prior segregation in austenite of elements such as P, S, and N play an important role in this kind of embrittlement [9]. The grain boundary carbides are thought to provide an effective barrier for slip blockage; they may also further increase the concentrations of intergranular impurities by rejection of solutes as the carbides thicken [25,16].

The behavior in H_2 of one of the commercial steels is compared with that of the high purity steel in Figure 7. It is evident that the systematic variation in Charpy notch toughness in the commercial steel with increasing tempering temperature is not reflected in a similar systematic variation in K_{th}. This suggests that the impurity concentrations in the grain boundaries are mainly inherited from the austenite and do not increase significantly with low temperature tempering. The toughness variation may be primarily due to changes in the carbide morphology. At this point we view the differences in the v-K curves in the commercial steel as non-systematic experimental scatter. Apparently K_c is close enough to K_{th} that Stage II tends to be ill-defined. The magnitude of the impurity effect is demonstrated by the enormous increase in K_{th} when the high purity steel is tested under conditions identical to those used for the commercial steel. Here also, the fracture mode in H_2 is cleavage, as opposed to microvoid coalescence in air, whereas the H_2-induced fracture mode in the impure steels is mostly intergranular.

The specific impurities which induce one-step temper embrittlement in the commercial steels appear to be mainly P and N [21]. The amounts required

at such a high strength level (1380 MPa) are quite small and are close to the limits of resolution of the Auger spectrometer. It is not yet possible to be quantitative about the P and N concentrations, but it is certain that these elements are present.

BRITTLE FRACTURE MODEL

We wish to consider a model which could ultimately become quantitative and which would employ experimentally measurable quantities to give criteria for brittle fracture, including the effects of both mobile and immobile solutes which lower cohesive strength. For simplicity we initially treat the hydrogen effect as simply additive to the other impurity effects. Impurity-hydrogen interactions, if they exist, can, in principle, be accommodated. For purposes of discussion, schematic plots with a scale of 10^5 PSI will be drawn to represent either a high strength steel with yield strength σ_y equal to 690 MPa (10^5 PSI) or an ultra high strength with σ_y = 1380 MPa (2 x 10^5 PSI).

Continuum Model of the Crack Tip Stress Field

Consider how the maximum principal stress σ_1 in the region around a crack tip in a stressed body varies with successive increments of nominal stress σ_{nom}. Initially the body remains elastic, and the maximum value of σ_1 is given by the Inglis solution [27].

$$\sigma_{1_m} = \sigma_{nom} \ (1+2\sqrt{a/\rho}) \qquad (1)$$

where a is the crack length and ρ is the crack tip radius. If ρ is taken to be a few μm, then the stress intensification factor could easily be 10^2. Thus, σ_{1m} rises very steeply with small increments of σ_{nom}. When σ_{1m} reaches σ_y, a plastic zone forms, and σ_1 is then bounded by this value at the free surface. Upon further increase in σ_{nom} the plastic zone grows larger; σ_1 then rises steeply beyond the crack tip due to the surrounding elastic region, and it passes through a maximum at some distance ahead of the crack [28]†. Finally, σ_{1m} reaches its limiting value of $\sim 3\sigma_y$. The progressive increase in σ_1 with increasing σ_{nom} is depicted schematically in Figure 8a. The maximum value of σ_1 ($=\sigma_{1m}$) must vary as shown in Figure 8b; the initial slope is $(1+2\sqrt{a/\rho})$ and the asymptotic limit is $\sim 3\sigma_y$.

Relation of Crack Tip Stresses to Fracture Strength

The cohesive strength of the Fe lattice σ_o^* is of order E/10 [29], 30×10^5 PSI ~ 20 GNm^{-2}. There is ample experimental evidence [9] that a local increase in impurity concentration, as in a grain boundary, can cause a reduction in cohesive strength, σ^*, which we designate by $\Delta\sigma_i^*$, and that concentrated hydrogen can also provide a reduction, which we call $\Delta\sigma_H^*$. The cohesive strength can be approximated [29] by

$$\sigma_o^* \simeq \left(\frac{E\gamma_o}{a_o}\right)^{1/2} \qquad (2)$$

†We make the approximation that an elliptical crack of large a and very small ρ will have essentially the same elastic-plastic stress field as a sharp crack, to which the analysis of Reference [28] applies.

boundaries also became enriched in N and P, as well as Ni and Mn. The latter two elements are believed to act as promoters of segregation of embrittling elements by cosegregation (cf. Table 1), rather than as embrittling elements themselves [9].

The effects of the variation of grain boundary composition on the v-K curve are shown in Figure 4. Values of K_{th} and v_{II} are strongly affected; v_{II} is taken to be the region of the first inflection in the steeply-rising v-K curve above K_{th}. As shown in Figure 5 K_{th} decreases and v_{II} increases, with increasing ageing time. It is important to note that the mode of cracking in hydrogen in the unembrittled steel is cleavage, as opposed to the microvoid coalescence found in air. That is, H_2 promotes cleavage fracture when impurity effects are absent.

Ultra High Strength Steels

As the prototypical material in this category we have chosen the often-studied 4340-type steel [21]. Here the impurity effects manifest themselves in what is perhaps most aptly referred to as one-step temper embrittlement [22]. A toughness trough occurs in the room temperature fracture energy of a notched-bar impact specimen when plotted against the temperature of tempering (which is the one embrittlement step). Figure 6 illustrates the toughness troughs in 4 different commercial heats of 4340 steel, and the absence of such a trough in a 4340-type high purity vacuum-induction melted steel which received the same heat treatment and had the same strength. The toughness troughs in the commercial steels were accompanied by corresponding peaks in the amount of intergranular fracture; only a very small amount of intergranular fracture could be produced in the high purity steel. It is well established that the onset of the trough coincides with the formation of M_3C carbides [23,24]. Apparently the tendency for impurity-induced intergranular fracture (which also occurs in as-quenched impure steels) is accentuated by carbide formation in the prior austenitic grain boundaries. It is thought that prior segregation in austenite of elements such as P, S, and N play an important role in this kind of embrittlement [9]. The grain boundary carbides are thought to provide an effective barrier for slip blockage; they may also further increase the concentrations of intergranular impurities by rejection of solutes as the carbides thicken [25,16].

The behavior in H_2 of one of the commercial steels is compared with that of the high purity steel in Figure 7. It is evident that the systematic variation in Charpy notch toughness in the commercial steel with increasing tempering temperature is not reflected in a similar systematic variation in K_{th}. This suggests that the impurity concentrations in the grain boundaries are mainly inherited from the austenite and do not increase significantly with low temperature tempering. The toughness variation may be primarily due to changes in the carbide morphology. At this point we view the differences in the v-K curves in the commercial steel as non-systematic experimental scatter. Apparently K_c is close enough to K_{th} that Stage II tends to be ill-defined. The magnitude of the impurity effect is demonstrated by the enormous increase in K_{th} when the high purity steel is tested under conditions identical to those used for the commercial steel. Here also, the fracture mode in H_2 is cleavage, as opposed to microvoid coalescence in air, whereas the H_2-induced fracture mode in the impure steels is mostly intergranular.

The specific impurities which induce one-step temper embrittlement in the commercial steels appear to be mainly P and N [21]. The amounts required

at such a high strength level (1380 MPa) are quite small and are close to the limits of resolution of the Auger spectrometer. It is not yet possible to be quantitative about the P and N concentrations, but it is certain that these elements are present.

BRITTLE FRACTURE MODEL

We wish to consider a model which could ultimately become quantitative and which would employ experimentally measurable quantities to give criteria for brittle fracture, including the effects of both mobile and immobile solutes which lower cohesive strength. For simplicity we initially treat the hydrogen effect as simply additive to the other impurity effects. Impurity-hydrogen interactions, if they exist, can, in principle, be accommodated. For purposes of discussion, schematic plots with a scale of 10^5 PSI will be drawn to represent either a high strength steel with yield strength σ_y equal to 690 MPa (10^5 PSI) or an ultra high strength with σ_y = 1380 MPa (2 x 10^5 PSI).

Continuum Model of the Crack Tip Stress Field

Consider how the maximum principal stress σ_1 in the region around a crack tip in a stressed body varies with successive increments of nominal stress σ_{nom}. Initially the body remains elastic, and the maximum value of σ_1 is given by the Inglis solution [27].

$$\sigma_{1_m} = \sigma_{nom} \left(1+2\sqrt{a/\rho}\right) \qquad (1)$$

where a is the crack length and ρ is the crack tip radius. If ρ is taken to be a few μm, then the stress intensification factor could easily be 10^2. Thus, σ_{1_m} rises very steeply with small increments of σ_{nom}. When σ_{1_m} reaches σ_y, a plastic zone forms, and σ_1 is then bounded by this value at the free surface. Upon further increase in σ_{nom} the plastic zone grows larger; σ_1 then rises steeply beyond the crack tip due to the surrounding elastic region, and it passes through a maximum at some distance ahead of the crack [28]†. Finally, σ_{1_m} reaches its limiting value of $\sim 3\sigma_y$. The progressive increase in σ_1 with increasing σ_{nom} is depicted schematically in Figure 8a. The maximum value of σ_1 ($=\sigma_{1_m}$) must vary as shown in Figure 8b; the initial slope is $(1+2\sqrt{a/\rho})$ and the asymptotic limit is $\sim 3\sigma_y$.

Relation of Crack Tip Stresses to Fracture Strength

The cohesive strength of the Fe lattice σ_o^* is of order E/10 [29], 30x10^5 PSI $\sim$20 GNm^{-2}. There is ample experimental evidence [9] that a local increase in impurity concentration, as in a grain boundary, can cause a reduction in cohesive strength, σ^*, which we designate by $\Delta\sigma_I^*$, and that concentrated hydrogen can also provide a reduction, which we call $\Delta\sigma_H^*$. The cohesive strength can be approximated [29] by

$$\sigma_o^* \simeq \left(\frac{E\gamma_o}{a_o}\right)^{1/2} \qquad (2)$$

†We make the approximation that an elliptical crack of large a and very small ρ will have essentially the same elastic-plastic stress field as a sharp crack, to which the analysis of Reference [28] applies.

where γ_o is the free energy of the relevant fracture surface, and a_o is the lattice parameter. A solute which lowers γ by $\Delta\gamma$ would reduce σ^* to

$$\sigma_i^* = \sigma_o^* \left(1 - \frac{\Delta\gamma}{\gamma_o}\right)^{1/2} \tag{3}$$

Hondros [30] has measured the effect of P on the free surface and grain boundary free energies of bcc Fe, and the maximum $\Delta\gamma$ he observed was of order 50 pct†. From equation (3) this would produce a $\Delta\sigma_i^*$ of 30 pct, which would be a substantial reduction. Even assuming an equivalent contribution by hydrogen, there could still be a significant gap between the maximum possible value of σ_i and the lowest value of σ^*. This is illustrated schematically by Figure 9.

Contribution of Dislocations

To account for the observation of brittle cracking it is necessary to invoke the classical concept of the pile-up of dislocations at the head of a blocked slip band and to superimpose the resultant stress on that obtained from continuum theory. To do this we must consider the events which must occur in the region of maximum stress in the plastic zone at the crack tip. The variation of the three principal stresses with distance from the crack tip is shown schematically [31] in Figure 10a. In the region of the maxima there must exist a point where a slip band is blocked by a carbide platelet on a grain boundary (cf. Figure 10b and c). (The carbide behaves elastically and therefore prevents plastic relaxation by slip at the head of the dislocation pile-up). The pile-up is of length L and contains n dislocations; the effective shear stress acting on the pile-up is

$$\tau = \frac{(\sigma_{1_m} - \sigma_{2_m})}{2} - \tau_f \tag{4}$$

where τ_f is a friction stress having a thermal component due to barriers such as particles and a temperature-dependent component due to barriers which can be overcome by thermal activation, such as the Peierls stress.

Eshelby et al. [32] have shown that

$$n \simeq \pi \frac{\tau}{G} \frac{L}{b} \tag{5}$$

where b is the Burgers vector and G is the shear modulus; the concentrated shear stress at the head of the pile-up is $n\tau$ [33].

The local shear stress $n\tau$ is treated as an additional state of pure shear which can be superimposed on the field of σ_1 and σ_2. Thus, it contributes an additional component of normal stress [34] across the carbide-matrix interface equal to $n\tau$, as shown in Figure 10c. The total stress on the interface is thus

$$\tilde{\sigma_{1_m}} = \sigma_{1_m} + n\tau = \sigma_{1_m} + \frac{\pi}{G}\left[\frac{\sigma_{1_m} - \sigma_{2_m}}{2} - \tau_f\right]^2 \frac{L}{b} \tag{6}$$

†The measurement was made at ~1700 K; the bulk concentration of P was almost 0.4 pct.

The upper bound on $\tilde{\sigma_{1_m}}$ can be evaluated for the plane strain condition in which strain hardening is neglected, since in this limiting case the maxima are given by [35]:

$$\sigma_{1_m} = \frac{(2+\pi)}{\sqrt{3}} \sigma_y \tag{7}$$

$$\sigma_{2_m} = \frac{\pi}{\sqrt{3}} \sigma_y \tag{8}$$

$$\sigma_{3_m} = \frac{(\sigma_{1_m} + \sigma_{2_m})}{2} = \frac{(1+\pi)}{\sqrt{3}} \sigma_y \tag{9}$$

Hence, equation 6 becomes

$$(\tilde{\sigma_{1_m}})_{\text{LIMIT}} = \frac{(2+\pi)}{\sqrt{3}}\sigma_y + \frac{\pi}{G}\frac{L}{b}\left[\frac{\sigma_y}{\sqrt{3}} - \tau_f\right]^2 \tag{10}$$

Therefore, by superimposing the continuum and dislocation stresses we find that the curve of σ_{1_m} versus σ_{nom} is displaced upward from that shown previously for the continuum alone (cf. Figure 8), as indicated by Figure 11.

Criterion for Brittle Cracking

Brittle cracking must occur when σ_{1_m} equals the effective value of σ^*, or

$$\sigma_o^* - \Delta\sigma_i^* - \Delta\sigma_H^* = \tilde{\sigma_{1_m}} \tag{11}$$

To examine the feasibility of fulfilling this criterion we can compare the upper bound of $\tilde{\sigma_{1_m}}$ for various values of σ_y with the probable values of σ^*. (τ_f is taken to be 10^4 psi for purposes of illustration). This is done in Figure 12, which illustrates that the pile-up length L is an important parameter. As σ_y increases, or as impurity-induced intergranular embrittlement (signified by $-\Delta\gamma$) increases, the pile-up length needed to induce a brittle crack decreases. For example, if σ_y is 10^5 PSI, and there is no intergranular embrittlement, an $L \simeq 4200$ b is needed to nucleate a crack. However, if σ_y is 2×10^5 PSI and γ is reduced by only 10 pct, an L of only 700 b is needed.

The effect of temperature in an unembrittled steel is indicated by Figure 13a. At temperature T_2 the yield strength is too low, and $\tilde{\sigma_{1_m}}$ never reaches σ_o^*; hence, fracture can occur only by microvoid coalescence. A decrease in temperature to T_1 produces enough elevation in σ_y to allow a brittle crack at $K = K_c$. From Figure 12 it is clear that such a tough-to-brittle transition could also be produced by an increase in L, which in mild steel is a function of grain size, as demonstrated by Low [36].

Impurity effects are added in Figure 13b. A small amount of intergranular embrittlement $\Delta\sigma_{i_1}^*$ is insufficient to permit brittle cracking at temperature T_2. However, further embrittlement to the extent of $\Delta\sigma_{i_2}^*$ is sufficient, and the tough-to-brittle transition is raised above T_2.

To account for the effect of hydrogen, we make the assumption, following Oriani and Josephic [37], that the reduction in cohesive strength by hydrogen $\Delta\sigma_H^*$ is proportional to the local hydrogen concentration C_H

$$\Delta\sigma_H^* \propto C_H \tag{12}$$

The local value of C_H at equilibrium can be calculated from the equation of Li et al. [38].

$$\ln \frac{C_H}{C_o} = \frac{\Omega\Theta}{RT} \tag{13}$$

where C_o is the equilibrium hydrogen concentration in the unstressed lattice†, Ω is the molar volume of hydrogen in Fe, and Θ is the hydrostatic tension

$$\Theta = \frac{\sigma_1 + \sigma_2 + \sigma_3}{3} \tag{14}$$

The value of Θ can, in principle, be calculated as a function of K if a solution for σ_{1m}, σ_{2m}, and σ_{3m} can be obtained for the region around a crack tip. The curve of σ_{1m} versus σ_{nom} must have the shape indicated in Figure 8b; we will assume that σ_{2m} and $\sigma_{3m} = 1/2(\sigma_{1m} + \sigma_{2m})$ have a similar shape. This would mean that C_H, which increases exponentially with Θ (cf. equation (13)),†† would increase very rapidly with K. Hence, $\Delta\sigma_H^*$ should do likewise, as indicated by Figure 13c. The point of intersection of σ^* and σ_{1m} represents a threshold value of K; this is the lowest K value at which hydrogen-induced crack extension can occur, since the solid σ^* curve represents the maximum hydrogen concentration.

The hydrogen concentration in the region of σ_{1m} is, of course, a function of time (as well as temperature and external hydrogen pressure). The dashed σ^* curves in Figure 13c are drawn to indicate that cracking occur in shorter times (i.e., higher cracking rates) at higher levels of K.

The superposition of impurity and hydrogen effects is indicated by Figure 13d. It is apparent that increasing reductions in cohesion by impurities, i.e., increasing $\Delta\sigma_i^*$, should lead to reduced K thresholds for hydrogen-induced cracking and to larger cracking rates at any $K > K_{th}$. This is consistent with our experimental results.

†Oriani and Josephic [37] suggested that C_o may be several orders of magnitude greater in a grain boundary than in the lattice. This would imply that hydrogen-induced cracking would tend to be intergranular, even in a pure steel. We have found that, as purity increases, the cracking mode shifts toward cleavage. Hence, the elevation of C_o in a pure grain boundary may be of secondary importance; in any case, we neglect it here.

††For example, using equation (13) for a high strength steel with $\sigma_y = 10^5$ psi, $\Theta_m = (1+\Pi)\ \sigma_y = 1.6\times10^{10}$ dynes/cm^2, at full constraint and using $\Omega = 2$cm^3/mole as the atomic volume of H in α-Fe [37] and taking T=300K, R=8.32x10^7 ergs/mole ^oK, we find that $C_H/C_o \simeq 4$ as the hydrogen enrichment factor due to lattice expansion in the region of maximum Θ. For an ultra high strength steel with $\sigma_y = 2\times10^5$ psi the enrichment factor is almost 14.

The model just described is an attempt to construct a simple conceptual framework for the analysis of hydrogen and impurity effects. It aims to provide a rationale for K_{th} and the steeply rising v above K_{th}. In principle, on this basis K_{th} could be calculated if we had an accurate stress analysis and good values for L, the pile-up length, τ_f, the friction stress, and C_o (T,p), the equilibrium hydrogen concentration in the matrix and in grain boundaries in Fe as a function of temperature and pressure. Even without knowledge of these parameters, however, experimental values of K_{th} for intergranular cracking in specimens of varying grain boundary composition can be used to determine whether the hydrogen-impurity interactions are additive or synergistic. As an example of the latter, the presence of a specific impurity in grain boundaries might raise the local C_o, due to an attractive interaction between the impurity and hydrogen.

It would be expected that the v-K curve would tend to level-off when the crack propagation rate becomes limited by the rate of diffusion of hydrogen to the region of maximum lattice expansion (i.e., maximum Θ). However, it seems unreasonable to expect that a K-independent regime of (constant) velocity should ensue, because hydrogen-assisted cracking occurs not by a smooth, uniform advance of a well-defined crack front, but rather by formation of small cracks in advance of the main crack and the subsequent joining of the small cracks with the main crack [20]. The small advance cracks often form along side of, rather than directly ahead of, the main crack, and this discontinuous crack advance occurs in an uneven way along the main crack front [20]. Therefore, when one determines a change in "crack" length by measuring a decrease in load or increase in crack opening displacement (knowing the specimen compliance as a function of crack length), or by other methods such as measuring changes in electrical resistance, one is actually dealing with the advance of a very complicated, discontinuous, uneven crack as if it were a relatively smooth, continuous crack, as produced, for example, by fatigue. Thus, in the actual case there are variations along the crack front of important parameters such as the state of stress and the diffusion distance of hydrogen to the region of maximum Θ. For such reasons it would appear rather presumptuous to be anything but qualitative about the v-K curve in Stage II. However, it seems reasonable that, as the impurity content of the grain boundaries increases, the velocity range where the leveling off tendency is observed should increase, since less hydrogen would be required to bring the σ^* and σ_{1m} curves into coincidence. This is consistent with Figure 4.

The basic ideas used in this model include those of Troianno and co-workers [40] and Oriani [41]. These are that hydrogen diffuses to the region of maximum Θ and there acts to lower cohesion and enables the formation of an integral crack. It must be admitted that the location of the initial crack at the point of maximum Θ has not been experimentally proven, although support for it does exist [40]. The possibility remains that initial cracking could occur closer to the crack tip; in this case the analysis given here would not be directly applicable. This area remains an important topic for future experiments.

Effects of Temperature and Pressure

Variations in temperature and pressure can have profound effects on the rate of hydrogen-induced cracking and on the threshold K value [18]. The expected effects can be enumerated as follows:

Temperature:

1. Controls the rate at which hydrogen can diffuse through the Fe lattice to the region of σ_{1m}.
2. Influences the tendency of gas molecules to adsorb on a free surface; this may account for the precipitous drop in cracking rate observed with increasing temperature [39].
3. Is the main extrinsic determinant of σ_y in a ferritic steel; this becomes less significance as σ_y is raised by intrinsic strengthening mechanisms.

Pressure:

1. Controls C_o, as indicated by Sievert's law; an increase in p_{H_2} leads to an increase in $C_o \propto p_{H_2}^{1/2}$, thus an increase in $C_H = C_o \exp \Omega\Theta/RT$.
2. Influences the $\Delta\mu_H$ which drives the inward migration of hydrogen; an increase in p_{H_2} increases the adsorption and thus the rate of absorption.

Superposition of these factors can become quite complex, but careful experimentation can isolate the primary effects [18,37,39].

ACKNOWLEDGEMENTS

This work has been supported by the National Science Foundation under grant number DMR-74-14577. The results on ultra high strength steels are from research supported by the U.S. Naval Air Systems Command under contract number N000 19-75-C-0125. Discussions with Professor J. R. Rice and Drs. J. F. Knott and R. P. Gangloff were most helpful.

REFERENCES

1. RELLICK, J. R., McMAHON, C. J., Jr., MARCUS, H. L. and PALMBERG, P. W., Met. Trans., 2, 1971, 1492.
2. JOLLY, P. and GOUX, C., Mem. Sci. Rev. Met., 66, 1969, 605.
3. PICHARD, P., RIEU, J. and GOUX, C., Mem. Sci. Rev. Met., 70, 1973, 13.
4. McMAHON, C. J., Jr., FURUBAYASHI, E., OHTANI, H. and FENG, H. C., Acta. Met., 1977.
5. GUTTMANN, M., Surface Science, 53, 1975, 213.
6. MULFORD, R. A., McMAHON, C. J., Jr., POPE, D. P., and FENG, H. C., Met. Trans. A., Vol. 7A, 1976.
7. OHTANI, H., FENG, H. C. and McMAHON, C. J., Jr., Met. Trans. 5, 1974, 1061.
8. CIANELLI, A. K., FENG, H. C., UCISIK, A. H. and McMAHON, C. J., Jr., to be published.
9. McMAHON, C. J., Jr., Matls. Sci. Eng., 25, 1976, 233.
10. BRIANT, C. L. and BANERJI, S. K., Intl. Met. Rev., to be published.
11. ORIANI, R. A., in Fundamental Aspects of Stress Corrosion Cracking, Ed., R. W. Staehle, N.A.C.E., Houston, 1969, 32.
12. INOUE, T., in Grain Boundaries in Engineering Materials (4th Bolton Landing Conf.), Ed., J. L. Walter, et al., Claitor's Publ. Divn., Baton Rouge, 1975, 553.
13. WERT, C., Phys. Rev., Vol. 79, 1950, 601.

14. CABRAL, U. Q., HACHE, A. and CONSTANT, A., C. R. Acad. Sci., 260T, 1965, 6887.
15. YOSHINO, K. AND McMAHON, C. J., Jr., Met. Trans., 5, 1974, 363.
16. McMAHON, C. J., Jr., YOSHINO, K. and FENG, H. C., Intl. Conf. on Stress Corrosion Cracking and Hydrogen Embrittlement in Steels, Unieux-Firminy, June, 1973.
17. NOVAK, S. R. and ROLFE, S. T., J. Materials, 4, 1969, 701.
18. WILLIAMS, D. P. and NELSON, H. G., Met. Trans. 1, 1970, 63.
19. LOGINOW, A. W. and PHELPS, E. H., Mat. Symp. Pet. Mech. Eng. Conf., Dallas, 1974.
20. BRIANT, C. L., McMAHON, C. J., Jr. and FENG, H. C., to be published.
21. BANERJI, S. K., McMAHON, C. J., Jr. and FENG, H. C., to be published.
22. McMAHON, C. J., Jr., in Grain Boundaries in Engineering Materials, (4th Bolton Landing Conf.) Ed. J. L. Walter et al., Claitor's Publ. Divn., Baton Rouge, 1975, 525.
23. KLINGLER, L. J., BARNETT, W. J., FROHMBERG, R. P. and TROIANO, A. R., Trans. ASM Vol. 46, 1954, 1557.
24. LEMENT, B. S., AVERBACH, B. L. and COHEN, M., Trans. ASM, 46, 1954, 851.
25. KULA, E. B. and ANCTIL, A. A., J. of Matls. ASTM, Vol. 4, 1969, 817.
26. RELLICK, J. R., McMAHON, C. J., Jr., Met. Trans., Vol. 5, 1974, 1439.
27. INGLIS, C. E., Trans. Instr. Nav. Arch., 55, 1913, 219.
28. RICE, J. R. and JOHNSON, M. A., in Inelastic Behavior of Solids, Ed. M. F. Kanninen et al., McGraw-Hill, New York, 1970, 641.
29. OROWAN, E., Rep. Prog. Phys., 12, 1949, 815.
30. HONDROS, E. D., Proc. Roy. Soc. A, 286, 1965, 479.
31. KNOTT, J. F., Fundamentals of Fracture Mechanics, Butterworth, London, 1973, 32.
32. ESHELBY, J. D., FRANK, F. C. and NABARRO, F. R. N., Phil. Mag., 42, 1951, 351.
33. COTTRELL, A. H., Dislocations and Plastic Flow in Crystals, Oxford, 1953, 105.
34. KOEHLER, J. S., Phys. Rev., 85, 1952, 480.
35. RICE, J. R., J. Appl. Mech. 35, 1968, 379.
36. LOW, J. R., Jr., in Relation of Properties to Microstructure, ASM, Cleveland, 1953, 163.
37. ORIANI, R. A. and JOSEPHIC, P. H., Acta. Met. 22, 1974, 1065.
38. LI, J. C. M., ORIANI, R. A. and DARKEN, L. W., Z. Phys. Chem., 49, 1966, 271.
39. GANGLOFF, R. P. and WEI, R. P., Scripta Met. 8, 1974, 661.
40. TROIANO, A. R., Trans. ASM, 52, 1960, 54.
41. ORIANI, R. A., Bunsen-Gesellschaft Phys. Chem. 76, 1972, 848.

Table 1 Effects of various elements on impurity induced embrittlement of steels

H																	He
Li	Be											B	C	N	O	F	Ne
Na	Mg											Al	Si	P	S	Cl	A
K	Ca	Sc	Ti	V	Cr	Mn	Fe	Co	Ni	Cu	Zn	Ga	Ge	As	Se	Br	Kr
Rb	Sr	Y	Zr	Cb	Mo	Tc	Ru	Rh	Pd	Ag	Cd	In	Sn	Sb	Te	I	Xe
Cs	Ba	La	Hf	Ta	W	Re	Os	Ir	Pt	Au	Hg	Tl	Pb	Bi	Po	At	Rn
Fr	Ra	Ac	Th	Pa	U												

embrittling element

segregation enhancer

appears to increase grain boundary cohesion

cosegregates with embrittling elements

segregation inhibitor

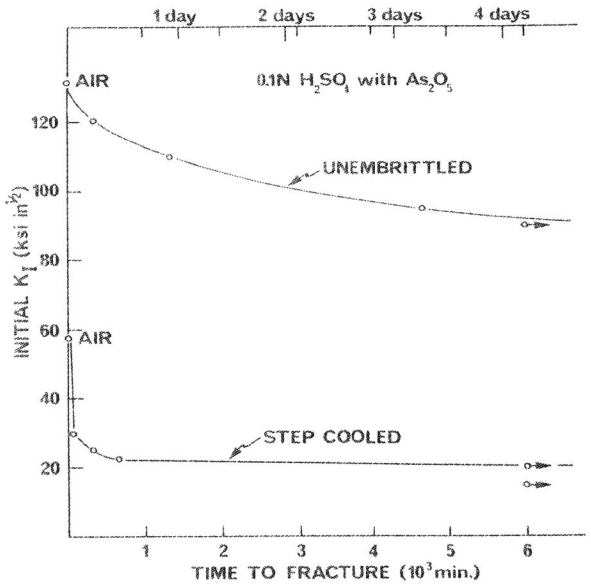

Figure 1 Effect of embrittlement by step cooling on the resistance to hydrogen-induced crack growth in HY130 steel. (Reference [15]).

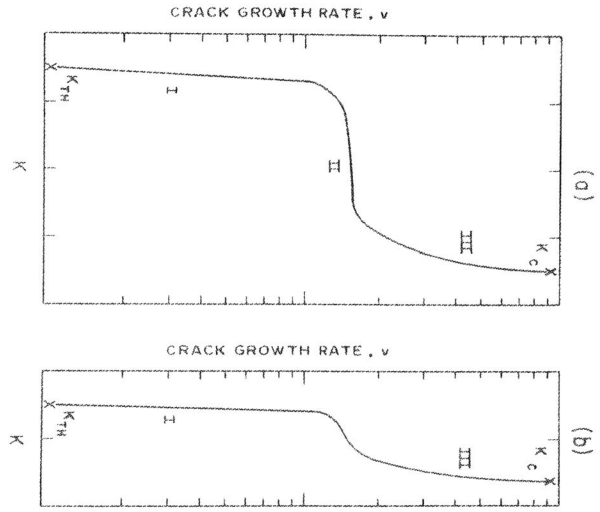

Figure 2 Schematic log v vs K curves showing (a) three stages and (b) suppression of stage II as K_c approaches K_{th}.

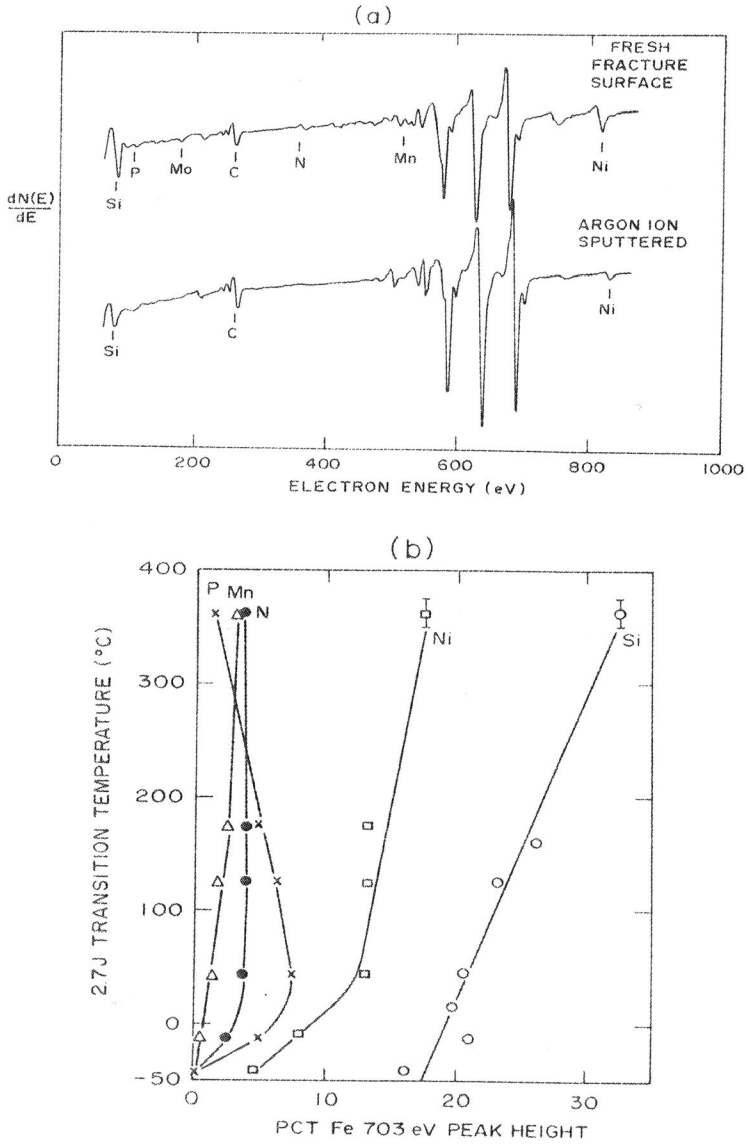

Figure 3 (a) Auger spectra from intergranular fracture surface of HY130 steel aged 3000 h at 753 K. (b) Variation of transition temperature with grain boundary composition as denoted by Auger peak heights. (Reference [20]).

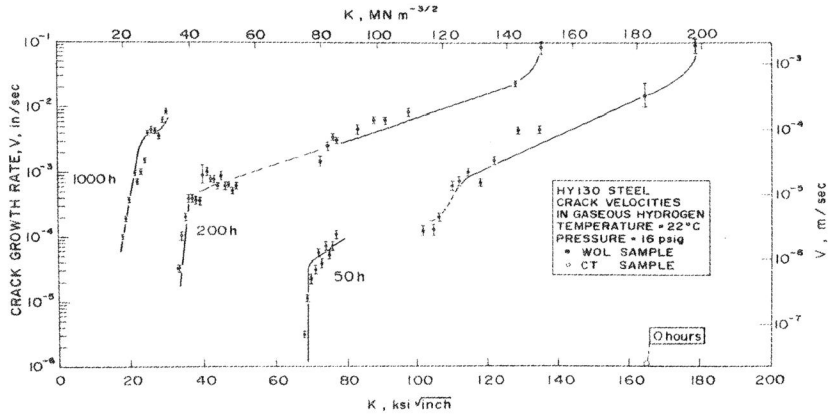

Figure 4 Effects of ageing time at 480°C on the log v vs K curve of HY130 steel tested in H_2 gas. (Reference [20])

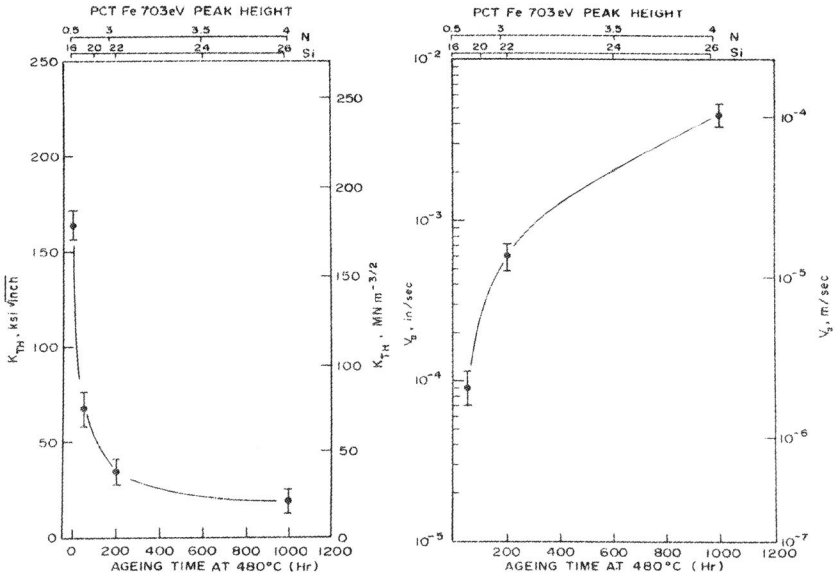

Figure 5 Variation of (a) v_{II} and (b) K_{th} with ageing time in HY130 steel tested in H_2 gas at 22°C, 16 psig. (Reference [20])

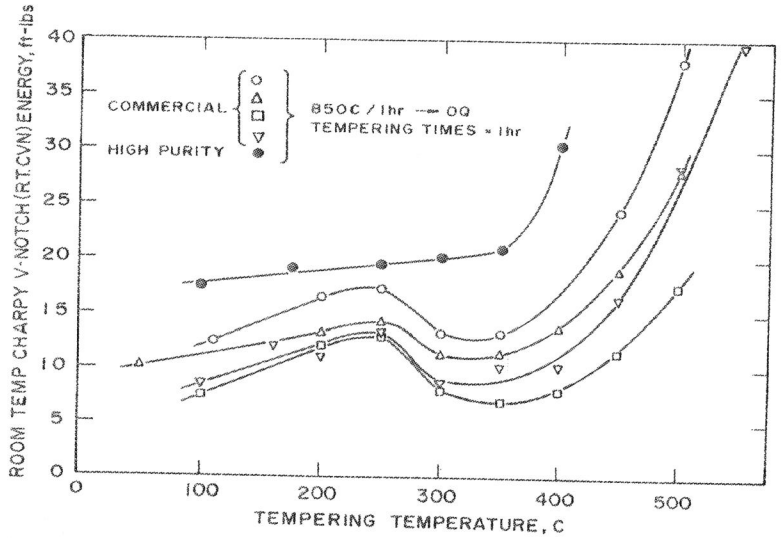

Figure 6 Variation of room temperature Charpy fracture energy with tempering temperature, showing toughness troughs in commerical 4340 steel in comparison with the monotonic increase in toughness in the high purity steel. (Reference [20])

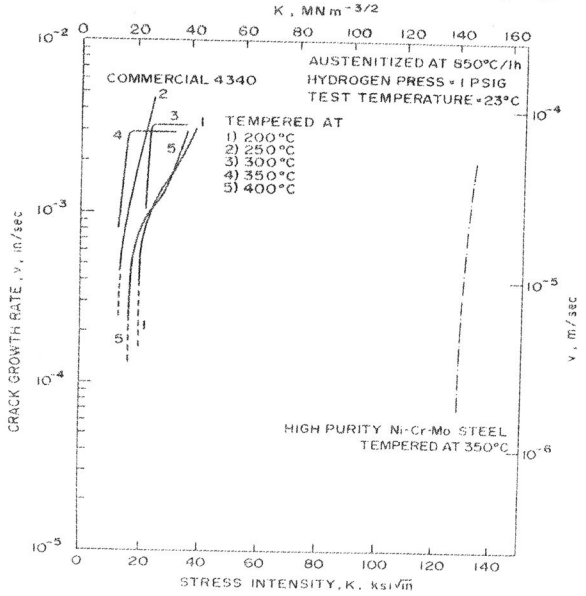

Figure 7 Comparison on log v vs K curves for a commercial 4340 steel tempered at various temperatures with that of the high purity steel. (Reference [20])

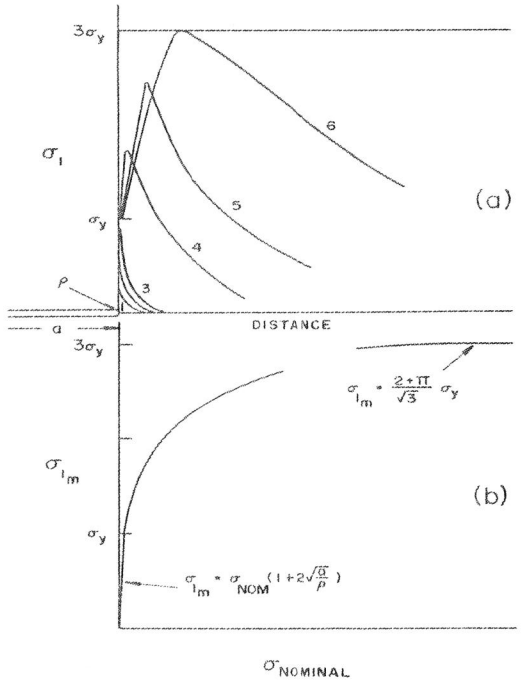

Figure 8 (a) Schematic representation of maximum principal stress σ_1 in region of crack tip at successively higher loading increments. (b) Maximum value of σ_1 ahead of crack as a function of nominal applied stress.

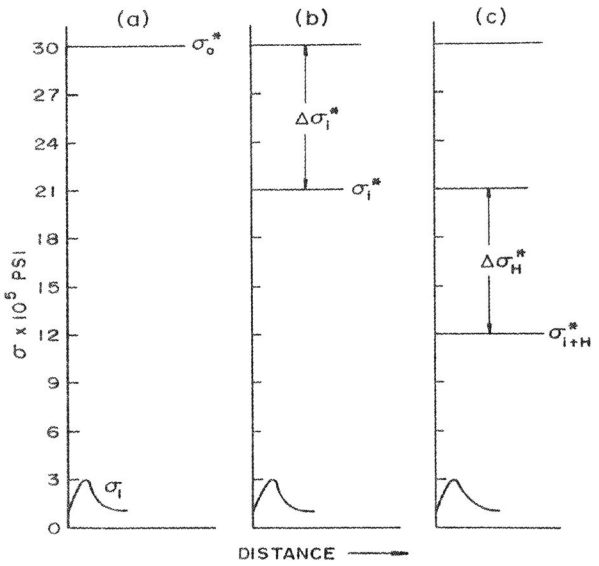

Figure 9 Relation of limiting value of σ_1 ahead of crack to the cohesive strength in (a) unembrittled steel, (b) embrittled steel and (c) embrittled steel with absorbed hydrogen.

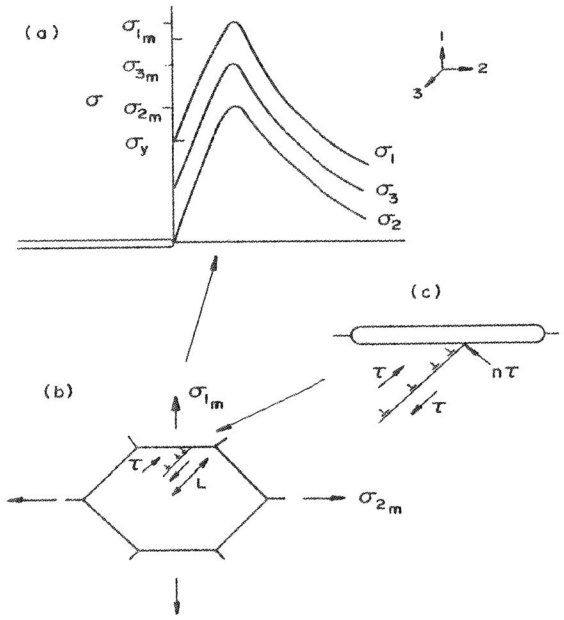

Figure 10 Schematic representation of (a) maximum principal stresses ahead of crack tip, (b) dislocation pile-up against grain boundary in region of maximum stress, and (c) grain boundary carbide acting as rigid barrier to the dislocation pile-up.

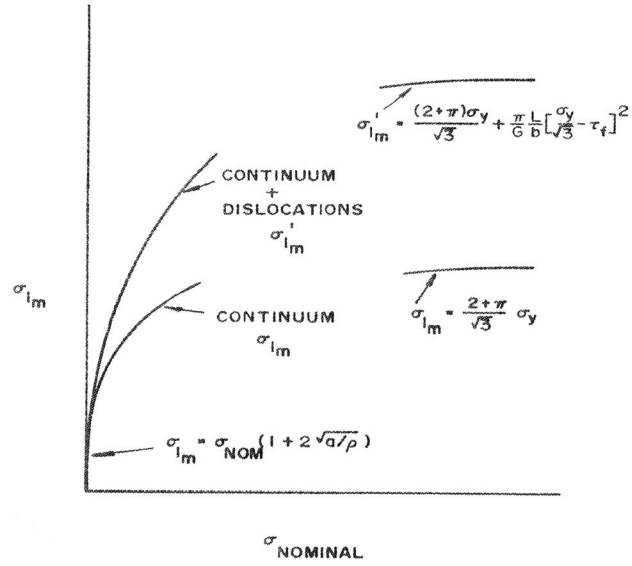

Figure 11 Variation of the maximum value of σ_1 ahead of crack with nominal applied stress as determined from continuum mechanics (σ_{1_m}) and from continuum plus dislocation mechanics (σ'_{1_m}).

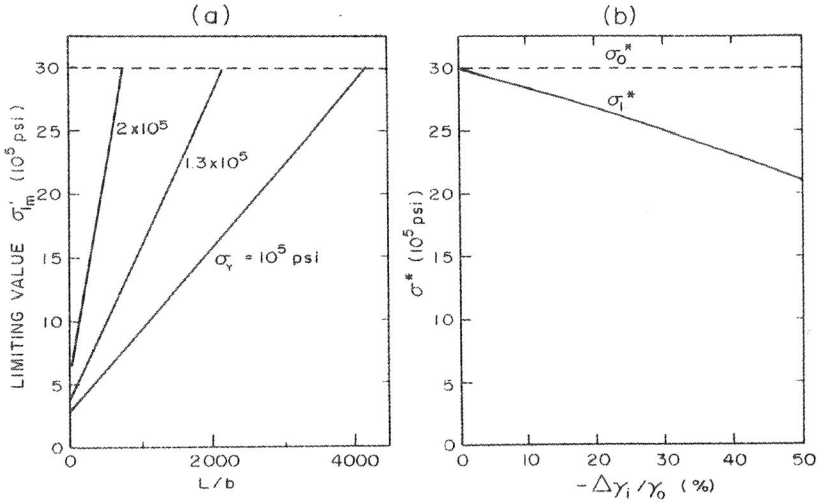

Figure 12 (a) Variation of σ'_{1_m} with pile-up length L for steels of various yield strength; τ_f taken as 10^4 psi. (b) Decrease in cohesive strength σ^* with reduction in surface free energy due to impurity segregation.

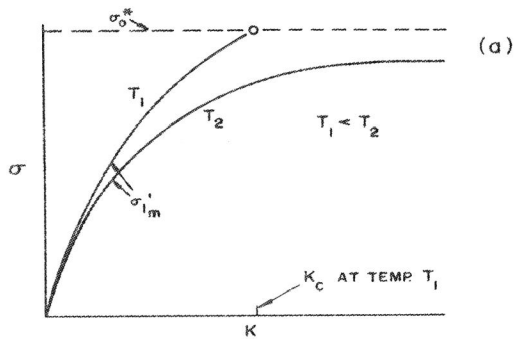

(a) Expected variation of σ'_{1_m} with applied K showing effect of elevation of σ_y as temperature is reduced, brittle fracture occurs at temperature T_1, but not T_2.

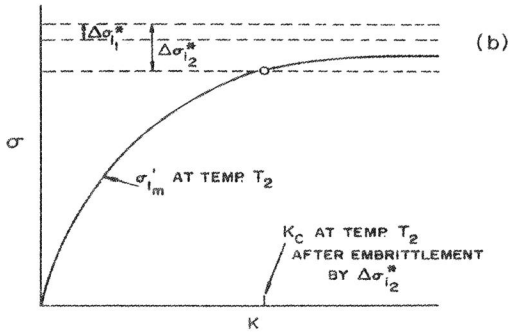

(b) Effect of impurity segregation in reducing intergranular cohesive strength and producing brittle fracture at temperature T_2.

Figure 13

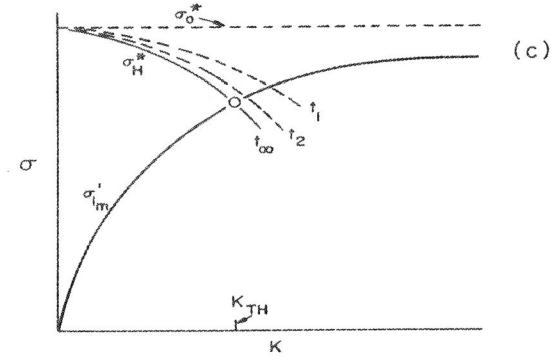

(c) Reduction of cohesive strength due to increased hydrogen accumulation with increasing applied K, leading to cracking at K_{th}. Cracking can occur in shorter times at higher K levels.

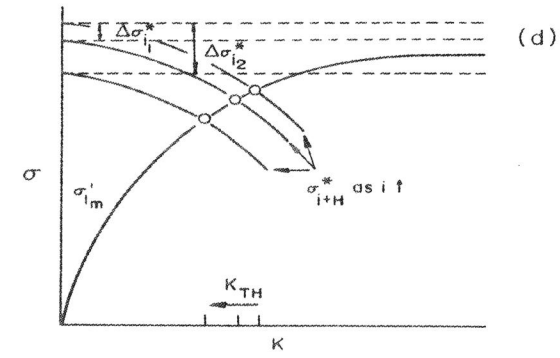

(d) Superposition of impurity and hydrogen effects; as impurity concentration increases K_{th} decreases and crack growth rate at $K>K_{th}$ increases.

Figure 13 (continued)